DOI: 10.15669/pnst.7.67

Progress in Nuclear Science and Technology
Volume 7 (2025) pp. 67-73

ARTICLE

Characterization of water Cherenkov neutron detector with high efficiency, availability, and affordability for nuclear security

Kosuke Tanabe [a, b], Masao Komeda [c], Yosuke Toh [c] and Hiroshi Sagara [a]

[a] Tokyo Institute of Technology, N1-17 2-12-1 Ookayama, Meguro-ku, Tokyo 152-8550, Japan; [b]National Research Institute of Police Science, 6-3-1 kashiwanoha, Kashiwa-shi, Chiba 277-0882, Japan: [c] Japan Atomic Energy Agency, 2-4 Shirakata, Tokai-mura, Naka-gun, Ibaraki 319-1195, Japan

To enhance nuclear security, rapid on-site detection of nuclear materials at any location is important, and the development of highly efficient and low-cost neutron detectors is strongly desired. Therefore, we have developed a water Cherenkov neutron detector (WCND) suitable for non-destructive assay methods for nuclear materials. In this study, characterization of the WCND was conducted through Monte Carlo simulations and test experiments using prototype detectors. The spatiotemporal characteristics of the electron fluxes were investigated, and the optical photon simulations indicated the discriminability between neutrons and gamma-rays using pulse height values. As a result of performance evaluation, the neutron detection efficiency was improved by a wavelength shifter, and a neutron detection efficiency equivalent to or better than that of Herium-3 detectors was experimentally obtained with the sufficient suppression of gamma-rays. Further improvements in detection efficiency and neutron/gamma-ray discrimination were expected by increasing the effective volume and number of photomultiplier tubes. The results showed that the WCND is a promising neutron detector with high efficiency, availability, and affordability for nuclear security.

Keywords: neutron detector; water Cherenkov detector; nuclear security; NDA; nuclear material

1. Introduction

In recent years, there has been a strong global demand to strengthen nuclear security to enable the prevention and response to illegal activities by non-state actors and terrorist organizations [1,2]. To ensure nuclear security, it is important to develop non-destructive assay (NDA) techniques for nuclear materials. Detecting fission neutrons emitted from spontaneous or induced fission reactions is extremely effective in detecting nuclear material. Although Helium-3 (He-3) proportional counters have been used primarily to detect fission neutrons from nuclear materials, the development of alternative detectors is strongly desired because of the recent global supply shortage of He-3 gas. The on-site detection of concealed nuclear materials at border control is an urgent issue, and neutron detectors with high efficiency, availability, and affordability are desired for NDA equipment to enhance nuclear security and safeguards [3].

Therefore, we have developed a water Cherenkov neutron detector (WCND) for the on-site detection of nuclear materials [4,5]. The WCND consists mainly of a water-filled container and photomultiplier tubes (PMTs), and it can be easily assembled in any size and at an extremely low cost. Gadolinium chloride ($GdCl_3$) is dissolved in water to increase neutron sensitivity. Water is readily available, leading to high availability and affordability. Therefore, similar to Boron-based or Lithium-doped detectors, the WCND is a strong candidate as an alternative to He-3 counters. Because the WCND is sensitive to both neutrons and gamma-rays, it can be used as a gamma-ray detector as well as a neutron detector. However, its high gamma-ray sensitivity is a drawback when used only as a neutron detector. Considering its application to NDA methods, such as an active neutron method [6,7], discrimination between neutrons and hydrogen-derived 2.223 MeV gamma-rays is essential. The detection of neutrons with sufficient suppression of gamma-rays will result in a promising alternative neutron detector.

When developing the WCND, it is important to investigate detailed characteristics, such as the response to neutrons and gamma-rays. In the present study, the characterization of the WCND was conducted by performing Monte Carlo simulations and test experiments using prototype detectors. The design goal of the WCND was to obtain a fission neutron detection efficiency of more than 3%, which was significantly high compared to conventional neutron detectors such as He-3 counters and liquid scintillators, while completely suppressing 2.223 MeV gamma-rays.

*Corresponding author. E-mail: tanabe@nrips.go.jp

2. Methodology

This section first describes the principle of water-based neutron detection, followed by simulation models to investigate the fundamental properties of WCND. Finally, an experimental setup using prototype detectors is described.

2.1. Principle of neutron detection using Cherenkov radiation

Incident neutrons are moderated in water and captured by the Gd nucleus, emitting gamma-rays of up to 8 MeV [8]. Compton scattering results in the emission of electrons, and Cherenkov light is emitted if electrons above 0.264 MeV pass through water. The number of Cherenkov photons is proportional to the range of electrons in water and is dominant in the short-wavelength region. The WCND is also sensitive to gamma-rays above 0.423 MeV because Cherenkov radiation is caused by the same process as neutrons. Therefore, it is essential to distinguish neutrons from gamma-rays to detect only neutrons. In this study, gamma-rays are suppressed at the trigger level by setting a threshold value for the light yield.

2.2. Monte Carlo simulation model

First, spatial and time distributions of the electron flux generated by the incidence of neutrons and gamma-rays were investigated using the PHITS code [9]. **Figure 1(a)** shows the simulation model. Neutrons and gamma-rays were vertically injected into the center of a side surface of the 100 × 100 × 100 cm water tank. The horizontal distribution (X-direction) and depth distribution (Z-direction) were calculated for electron flux values above 0.264 MeV generated in water. The number of mesh divisions for calculation in each direction was set to 100. To study the decay and capture times to the nucleus of neutrons in water, the time distribution of the electron flux was also calculated with the neutron incidence time set to 0 s. To examine the effect of Gd addition, $GdCl_3$ was dissolved in water with a concentration range of 0.0–1.0 wt%. The energy distributions of incident particles were set to monoenergetic neutron of 0.1 and 2.0 MeV and monoenergetic gamma-ray of 1.332 and 2.223 MeV, respectively.

Next, the light yield detected by PMTs and the detection efficiencies of neutrons and gamma-rays were examined using the Geant4 code [10]. All processes from the incidence of neutrons or gamma-rays to the generation and transport of Cherenkov light can be calculated by this code. As shown in Figure 1(a), 2-inch PMTs were placed on top of the acrylic container filled with pure water doped with 0.5 wt% of $GdCl_3$. The number of Cherenkov photons reaching the photocathode of PMT was defined as the light yield, and the effects of the effective volume (effective area: $X \times Y$, thickness: Z) of the radiation medium and the number of PMTs on the detection efficiency were investigated. The incident position and angle dependences of the detection efficiencies were also examined. The optical parameters of materials and the quantum efficiency of PMT were obtained from previous studies [4,5]. The reflective property at the boundary between acrylic and water was treated as diffuse reflections, and the reflectivity was set uniformly to 90% in the PMT sensitivity region.

2.3. Experimental setup for performance evaluation

In addition to the above simulations, experimental studies were performed. First, a small prototype detector (14.3 × 19.0 × 14.3 cm) was constructed, and then the effects of a wavelength shifter, detection efficiency, and neutron/gamma-ray (n/γ) discrimination were evaluated. Because Cherenkov light is dominant in the short-wavelength region, a wavelength shifter converting ultraviolet (UV) light into the PMT sensitivity region improves the light yield and n/γ discrimination [11]. The effect of carbostyril 124 (CS124) was examined using the prototype detector, one PMT (H11284-100, Hamamatsu [12]), and Cf-252 (7.6 kBq) and Co-60 (1.6 kBq) sources. The Co-60 source was used as a reference for setting the threshold value for n/γ discrimination because the threshold for suppressing the summed gamma-rays (1.173 + 1.332 = 2.505 MeV) from the Co-60 ensured suppression of the 2.223 MeV gamma-rays. A diffuse reflective material (Tyvek, 1060B, 0.172-mm thick) was attached to the inner surface of the detector. The $GdCl_3$ concentration was 0.5 wt%. The analog signal from the PMT was amplified, and the pulse height spectrum was obtained with a multichannel analyzer (MCA). The sources were set at the center of the detector side surface, and the measurement time was 10 min.

Subsequently, the position dependence of the detection efficiency was investigated using a large WCND (30 × 30 × 25 cm), four PMTs (H11284-100), and Cf-252 (5.1 MBq) and Co-60 (0.44 MBq) sources. A diffuse reflective material (PMR10P1, 0.75 mm-thick) was attached to the inner

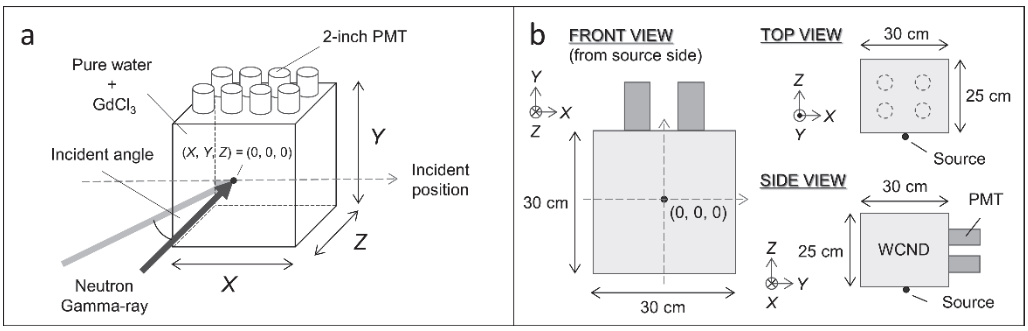

Figure 1. (a) Simulation model, (b) Experimental setup.

surface of the detector. **Figure 1(b)** shows the experimental setup. The gain of each PMT was adjusted using cosmic rays. After each analog signal was amplified and summed up, the pulse height spectrum was obtained by MCA. Considering the dead time, the trigger level for MCA data acquisition was set to 80 channels. The relative value of the detection efficiency was evaluated when the source position was changed in the horizontal (X) and vertical (Y) directions. Each measurement time was 2 min.

3. Numerical simulation results

3.1. Spatial and time distributions of electron flux

Figure 2(a) shows the depth distribution of the electron flux (above 0.264 MeV) from the detector surface at neutron and gamma-ray incidences. Regardless of the Gd concentration, the 2.0 MeV neutron-induced electron flux peaked at approximately 6.0 cm from the detector surface, and 42% of the electrons were generated within 10 cm and 70% within 20 cm. On the other hand, the gamma-ray-induced electron flux peaked at 1 cm from the surface and decreased exponentially with depth. Only the neutron-induced electron flux was increased by the addition of Gd, saturating at 0.5 wt%. This is because most of the neutrons were captured not by the hydrogen nuclei but by the Gd nuclei. For neutrons, the electron flux distribution shifted toward the deeper side with increasing energy. **Figure 2(b)** shows the X-directional distribution of the electron flux. More than 87% of the 2.223 MeV gamma-ray distribution was concentrated at ±2.0 cm, while 60% of the 2.0 MeV neutrons were distributed at ±10 cm and 81% at ±20 cm. The incidence of neutrons at the detector edge would decrease detection efficiency and discrimination owing to the decline in light yield. **Figure 2(c)** shows the time distribution of the electron flux. Neutrons of 2.0 MeV were incident into water with Gd concentrations of 0.1 and 0.5 wt%. The peak neutron capture time was at 7.0 µs, independent of the Gd concentration, and 73% of neutrons were captured within 20 µs at 0.5 wt%. If information on the incident time of the particles is available, the time difference from gamma-rays can be used to discriminate between neutrons and gamma-rays.

3.2. Detection efficiency

Figure 3 shows the result of the optical photon simulation using Geant4. Figure 3(a) shows the distribution of Cherenkov photon counts detected by PMTs when neutrons (2.0 MeV) and gamma-rays (8.0, 2.223, and 1.332 MeV) were incident into the detector. The number of photons on the horizontal axis corresponds to the light yield. The effective volume was 25 × 25 × 25 cm, and 16 of the 2-inch PMTs were placed on the top surface of the detector. The number of incidents of each particle was 10^6. By setting a threshold value and selecting events with light yield above the threshold, the discrimination between neutrons and gamma-rays can be expected. The light yield of gamma-rays increased with increasing energy, while that of neutrons was not energy dependent. For gamma-rays above 8 MeV, discrimination from neutrons by the pulse height value was theoretically impossible. Figure 3(b) shows the correlation between the detection efficiency and threshold value. Gamma-rays were suppressed with an increasing threshold, and a neutron detection efficiency of 16.1±0.1% was obtained at a threshold of 35 photons, suppressing 2.223 MeV gamma-rays. The error was statistical.

As a gamma-ray detector, the detection efficiency of 2.223 MeV gamma-rays was 17.8±0.1% at a threshold of 20 photons, at which 1.332 MeV gamma-rays were suppressed.

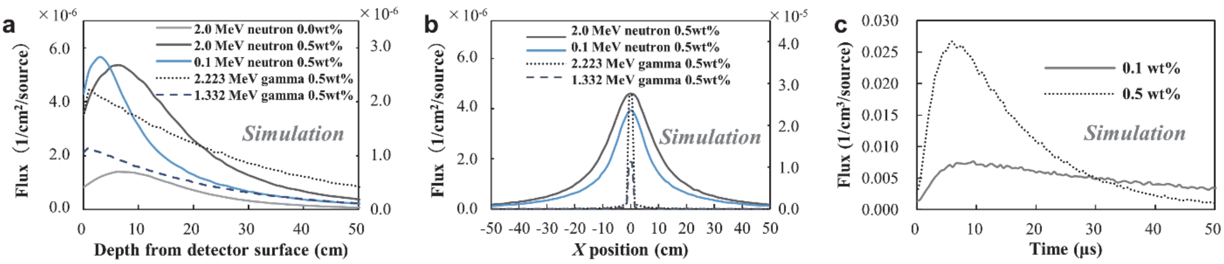

Figure 2. (a) Depth distribution of the electron flux, (b) X-directional distribution of the electron flux, (c) Time distribution of the electron flux. The right axes of (a) and (b) corresponding to the electron flux of gamma-rays.

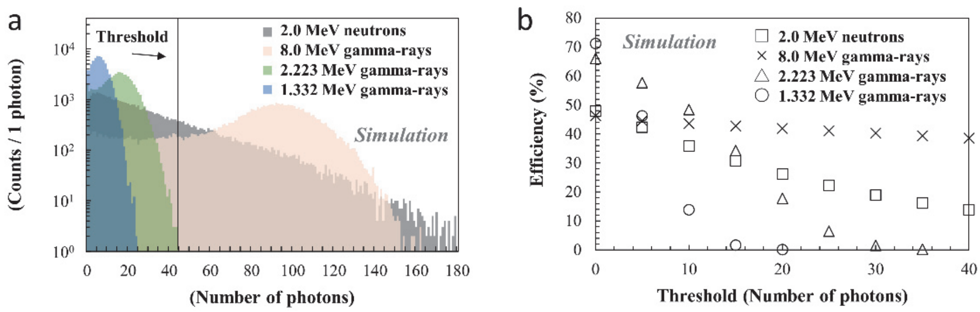

Figure 3. (a) Histogram of number of Cherenkov photons, (b) Correlation between detection efficiency and threshold value.

The threshold at which the detection efficiency became 10% was 23 photons, suppressing gamma-rays below 1.700 MeV. Therefore, to ensure a gamma-ray detection efficiency of more than 10%, energy selectivity of gamma-rays of approximately 500 keV was expected by using the pulse height discrimination.

3.3. Effective volume, position and angle dependences, effective area ratio of PMT

Figure 4(a) shows the correlation between the neutron detection efficiency and effective volume (effective area × thickness). If only the effective volume is increased while keeping the number of PMTs constant, the light collection efficiency will decrease. In this analysis, the top surface of the detector was uniformly defined as the photocathode. The threshold was set at a level that would suppress 2.223 MeV gamma-rays. With an increasing effective area, the discriminability between neutrons and gamma-rays improved and saturated at approximately 70 cm. This discriminability also increased with thickness, saturating at approximately 40 cm. These were generally consistent with the results presented in Figure 2.

Figure 4(b) and **4(c)** show the incident position and angle dependences of the detection efficiency. The effective volume was 50 × 50 × 40 cm, and 16 of the 2-inch PMTs were placed on top of the detector. The threshold was set at 10 photons. Compared with the detection efficiency of gamma-rays, that of neutrons was more position dependent, especially at the edge of the detector. The neutron detection efficiency at 5 cm from the edge of the detector decreased by 33% from the central position. With respect to the dependence on the incident angle, both the neutron and gamma-ray detection efficiencies decreased as the incident angle increased. The relative efficiencies at 60 degrees to 0 degrees were 0.68 for neutrons and 0.66 for gamma rays, respectively.

Table 1 shows the correlation between the neutron detection efficiency and the effective area ratio of PMT, which was defined as the ratio of the PMT photocathode to the detector surface area (total area of six surfaces). The effective volume was 50 × 50 × 40 cm, and PMTs were placed on top of the detector. The threshold was set to a level at which 2.223 MeV gamma-rays were suppressed. As the effective area ratio of PMT was increased, n/γ discrimination was improved. At the same effective volume, the neutron detection efficiency was significantly increased by the additional installation of PMT. The increase in the effective volume and number of PMTs becomes a bottleneck in terms of portability and cost. Therefore, it is desirable to optimize those factors according to the application and performance requirements.

4. Experimental results

4.1. Effect of wavelength shifter

Figure 5(a) shows the pulse height spectra for CS124 concentrations of 0.0 and 3.0 mg/L. The environmental background events were subtracted. The addition of CS124 increased the light yields dramatically for both neutrons and gamma-rays. The absorption wavelength peak of CS124 is observed at 340 nm, and the maximum emission wavelength is 417 nm [11]. Because the Cherenkov light in the UV region was converted into the sensitive region of the PMT, which was also transparent to the acrylic window, the number of detected photons was increased, leading to an improvement of the detection efficiency and discrimination. In the spectrum of 3.0 mg/L for Co-60, there were tail events caused by summed gamma-rays from Co-60 in the region of approximately 300 to 400 channels. **Figure 5(b)** shows the correlation between the detection efficiency and CS124 concentration at the threshold of 100 channels. The effect of CS124 became saturated at approximately 3.0 mg/L. Comparing the neutron detection efficiencies of 0.0 and 3.0 mg/L at the threshold of equal gamma-ray suppression, the addition of CS124 increased the neutron efficiency by a factor of 1.4.

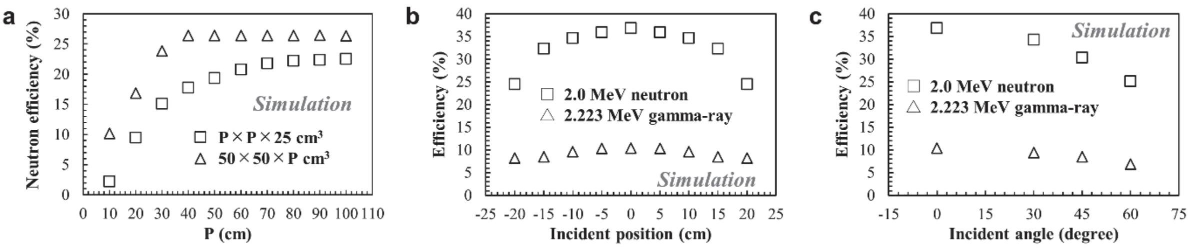

Figure 4. (a) Correlation between neutron detection efficiency and effective volume (effective area × thickness), (b) Incident position dependence of detection efficiency, (c) Incident angle dependence of detection efficiency.

Table 1. Correlation between neutron efficiency and effective area ratio of PMT.

Number of 2-inch PMTs	63	48	35	24	15	8
Effective area ratio of PMT (%)	9.82	7.48	5.46	3.74	2.34	1.25
Neutron efficiency (%)	26.8 ± 0.1	23.8 ± 0.1	22.1 ± 0.1	19.6 ± 0.1	18.1 ± 0.1	12.6 ± 0.1

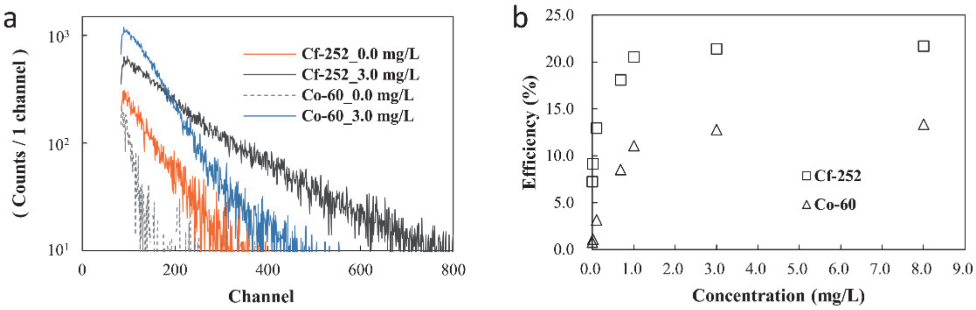

Figure 5. (a) Pulse height spectra for each CS124 concentration with the Cf-252 and Co-60 sources, (b) Correlation between detection efficiency and CS124 concentration at the threshold of 100 channels.

4.2. Detection efficiency and its position dependence

As shown in Figure 5(a), the neutron-induced light yield was larger than that of gamma-rays. Therefore, neutrons and gamma-rays were clearly distinguished by the pulse height value. The neutron detection efficiency was 5.2±0.1% at the threshold of 400 channels, which was sufficient to suppress summed gamma-rays from Co-60. The error was statistical. This result was in good agreement with the simulation results, and this neutron detection efficiency was equivalent to or better than the 2.6% efficiency of the He-3 detector bank in a previous study [4]. Furthermore, the detection efficiencies of neutrons and gamma-rays at the threshold of 150 channels were 16.5±0.1% and 5.0±0.1%, respectively. This result indicated that WCND is applicable not only as a neutron detector but also as a gamma-ray detector, and it demonstrates energy selectivity by selecting the threshold value.

Figure 6 shows the incident position dependence of the detection efficiencies of the large WCND. Relative efficiencies to the central position at the same threshold are shown. Owing to the absence of a collimator, this result includes the position and angle dependences indicated in Figure 4. For gamma-rays, the relative efficiency variation was within 5% in both directions. On the other hand, the neutron detection efficiency decreased toward the edge. In the horizontal direction, the relative efficiency decreased by 22% at ±11 cm from the center position (4 cm from the detector edge). This dependence was caused by the escaping of Gd prompt gamma-rays from the detector near the edge. Thus, when the threshold is adjusted for central incidence, the neutron detection efficiency decreases by approximately 20% at 5 cm from the edge. This dependence was an acceptable variation that did not directly affect the position dependence of nuclear material detection in the measured sample. While the horizontal direction showed symmetrical dependence, the vertical direction showed higher efficiency on the side closer to the connection surface of PMT. Because the effective area ratio of PMT for the detector was 1.69%, it is expected that increasing the number of PMTs will improve the detection efficiency and mitigate the position dependence.

5. Discussion

To enhance nuclear security, it is important to detect nuclear materials at various locations, especially at customs and border security. To achieve rapid detection at arbitrary locations by deploying nuclear material NDA devices globally, highly efficient, low-cost, and portable neutron detectors are optimum.

The experimental results obtained in this study revealed that using even a small WCND (14.3 × 19.0 × 14.3 cm) with one 2-inch PMT resulted in a neutron detection efficiency of 5.2±0.1%, suppressing the summed gamma-rays from Co-60. This performance was equivalent to or better than that of the He-3 detector in terms of sensitivity to fission neutrons [4]. Increasing the effective volume and number of PMTs was expected to improve the neutron detection efficiency by more than 20%. However, this would be a trade-off against portability and cost. Compared to the He-3 detector, the WCND does not require a moderator and allows measurements that suppress thermal neutrons by covering the detector with boron rubbers.

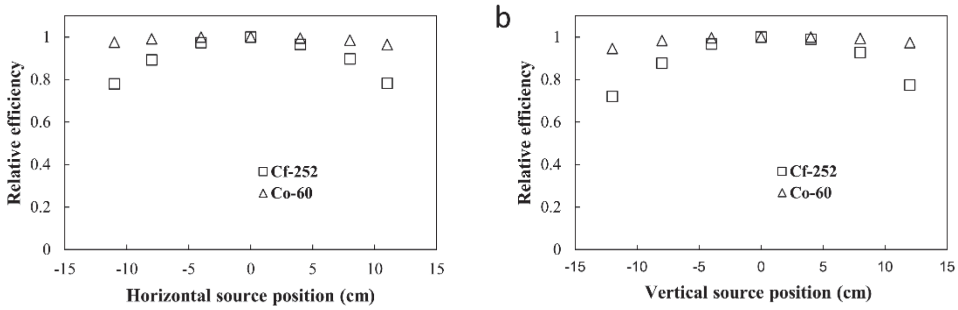

Figure 6. (a) Position dependence of relative efficiency (*X*-direction), (b) Position dependence of relative efficiency (*Y*-direction).

Moreover, the WCND can be easily fabricated in both large and small sizes, and has an extremely low production cost compared with other neutron detectors. Because WCNDs of any shape can be assembled, measurements with large three-dimensional (3D) angles can be realized by enclosing the measurement object with the detector. Furthermore, the WCND has high-portability because it can be operated to transport empty containers and obtain water on-site. Assuming the use of tap water on site, evaluations of the effects of impurities in the water should be performed in further studies.

Consequently, the WCND is a promising alternative neutron detector with high efficiency, availability, and affordability for nuclear security. In actual applications where gamma-rays below 2.223 MeV coexist, a neutron detection efficiency higher than a few percent was expected using WCND, regardless of the neutron-to-gamma-ray ratio. In addition to its high applicability as a neutron or gamma-ray detector for passive NDA methods [13], WCNDs are also expected to be applied to active NDA methods because the potential for the suppression of 2.223 MeV gamma-rays was demonstrated, which is a major background event during actual operation. In future studies, WCNDs with optimized designs should be developed for different applications and purposes, and their applicability and performance for each NDA method should be experimentally evaluated. In addition, changes of the wavelength shifter over time should be studied, assuming long-term operation.

6. Conclusion

In the present study, WCND characterization was conducted using Monte Carlo simulations and test experiments using prototype detectors. The calculated results revealed that the neutron-induced electron flux was distributed 81% in the horizontal range of ±20 cm and 70% within a 20 cm depth. On the other hand, the gamma-ray flux was locally distributed more than 87% in the horizontal range of ±2.0 cm. In addition, optical photon simulations indicated the discriminability between neutrons and gamma-rays using pulse height values. As a result of test experiments, CS124 improved the neutron detection efficiency by a factor of 1.4, and a neutron detection efficiency equivalent to or better than that of He-3 detectors was obtained, suppressing summed gamma-rays from Co-60. Further improvements in detection efficiency and discrimination were expected by increasing the effective volume and the number of PMTs. Moreover, the incident position and angle dependences were also evaluated and there was no contradiction in the dependence of experimental and computational results. The performance as a gamma-ray detector was also investigated, showing the energy selectivity by pulse height discrimination.

In summary, the WCND is a promising neutron detector with high efficiency, availability, and affordability for nuclear security. In future studies, we will develop WCNDs with optimized designs for different applications and purposes, and experimentally evaluate their applicability and performance for each NDA method.

Acknowledgements

This work was partially supported by JSPS KAKENHI Grant Numbers JP20K15213, JP24K17638, and Nuclear Regulation Authority, Japan.

References

[1] IAEA, Nuclear Security Systems and Measures for Major Public Events, *IAEA Nuclear Security Series* No 18 (2012).

[2] P.G. Martin, N.G. Tomkinson and T.B. Scott, The future of nuclear security: Commitments and actions – Power generation and stewardship in the 21st century, *Energy Policy* 110 (2017), pp. 325-330.

[3] IAEA, Nuclear Security Recommendations on Physical Protection of Nuclear Material and Nuclear Facilities (INFCIRC/225/Revision 5), *IAEA Nuclear Security Series* No13 (2011).

[4] K. Tanabe, M. Komeda, Y. Toh, Y. Kitamura, T. Misawa, K.Tsuchiya, et al., Development of a water Cherenkov neutron detector for the active rotation method and demonstration of nuclear material detection, *Journal of Nuclear Science and Technology* 60 (2022), pp. 769-781.

[5] K. Tanabe, M. Komeda, Y. Toh, Y. Kitamura, T. Misawa and H. Sagara, Verification of the Applicability of Water Cherenkov Detector to Active Neutron Method and Development of a Prototype Detector, *2021 IEEE Nuclear Science Symposium and Medical Imaging Conference (NSS/MIC)*, (2021), pp. 1-3.

[6] M. Komeda and Y. Toh, Conceptual study on a novel method for detecting nuclear material using a neutron source, *Annals of Nuclear Energy* 135 (2020), 106993.

[7] M. Komeda, Y. Toh, K. Tanabe, Y. Kitamura and T. Misawa, First demonstration experiment of the neutron rotation method for detecting nuclear material, *Annals of Nuclear Energy* 159 (2021), 108300.

[8] T. Tanaka, K. Hagiwara, E. Gazzola, A. Ali, I. Ou, T. Sudo, et al., Gamma-ray spectra from thermal neutron capture on gadolinium-155 and natural gadolinium, *Progress of Theoretical and Experimental Physics 2020* (2020), 043D02.

[9] T. Sato, Y. Iwamoto, S. Hashimoto, T. Ogawa, T. Furuta, S. Abe, et al., Features of Particle and Heavy Ion Transport code System (PHITS) version 3.02, *Journal of Nuclear Science and Technology* 55 (2018), pp. 684-690.

[10] S. Agostinelli, J. Allison, K. Amako, J. Apostolakis, H. Araujo, P. Arce, et al., Geant4–a simulation toolkit, *Nuclear Instruments and Methods in Physics Research Section A: Accelerators, Spectrometers, Detectors and Associated Equipment* 506 (2003), pp. 250–303.

[11] X. Dai, E. Rollin, A. Bellerive, C. Hargrove, D. Sinclair, C. Mifflin, et al., Wavelength shifters for water Cherenkov detectors, *Nuclear Instruments and Methods in Physics Research Section A: Accelerators, Spectrometers, Detectors and Associated Equipment*

589 (2008), pp. 290-295.
[12] Home | Hamamatsu Photonics n.d. https://www.hamamatsu.com/us/en.html (accessed June 9, 2023).
[13] R.T. Kouzes, E.R. Siciliano, J.H. Ely, P.E. Keller and R.J. McConn, Passive neutron detection for interdiction of nuclear material at borders, *Nuclear Instruments and Methods in Physics Research Section A: Accelerators, Spectrometers, Detectors and Associated Equipment* 584 (2008), pp. 383-400.